frontiers | Frontiers in Earth Science

TYPE Original Research
PUBLISHED 27 January 2023
DOI 10.3389/feart.2023.1048509

OPEN ACCESS

EDITED BY
Liang Zhang,
China University of Geosciences, China

REVIEWED BY
Jilong Han,
China University of Geosciences, China
Qingquan Liu,
Central South University, China
Binghan Chen,
Institute of Mineral Resources, Chinese Academy of Geological Sciences, China

*CORRESPONDENCE
Jun-Jian Li,
tjlijunjian@163.com
Zhi-Cai Dang,
dangzhicai@163.com

SPECIALTY SECTION
This article was submitted to Structural Geology and Tectonics, a section of the journal Frontiers in Earth Science

RECEIVED 19 September 2022
ACCEPTED 17 January 2023
PUBLISHED 27 January 2023

CITATION
Li J-J, Dang Z-C, Fu C, Zhang P-P, Tian J-P and He J-T (2023), Genesis of the Yangjiakuang gold deposit, Jiaodong peninsula, China: Constraints from S-He-Ar-Pb isotopes, and Sm-Nd and U-Pb geochronology.
Front. Earth Sci. 11:1048509.
doi: 10.3389/feart.2023.1048509

Genesis of the Yangjiakuang gold deposit, Jiaodong peninsula, China: Constraints from S-He-Ar-Pb isotopes, and Sm-Nd and U-Pb geochronology

Jun-Jian Li[1,2]*, Zhi-Cai Dang[1,2]*, Chao Fu[1,2], Peng-Peng Zhang[3], Jie-Peng Tian[4] and Jiang-Tao He[5]

[1]Tianjin Center, China Geological Survey, Tianjin, China, [2]North China Center for Geoscience Innovation, China Geological Survey, Tianjin, China, [3]Institute of Geophysical and Geochemical Exploration, Chinese Academy of Geological Science, Langfang, China, [4]School of Civil Engineering, Shandong Jianzhu University, Jinan, China, [5]Institute of Geological Surveying, Hebei GEO University, Shijiazhuang, China

Located in the Penglai-Qixia-Fushan Gold Belt, the Yangjiakuang gold deposit formed in the marble of the Paleoproterozoic Fenzishan Group is different from the previous altered rock-type gold deposits whose host gold-bearing rocks are Archean gneiss and Mesozoic granite. Two gold orebodies have been explored within the Yangjiakuang gold deposit, and both of them were controlled by the Yangjiakuang syncline. Three ore-forming stages have been recognized, including the pyrite-sericite stage (I), the gold, polymetallic sulfide, and quartz stage (II), and quartz-calcite stage (III). The calcites, which represent the main metallogenic stage (II) at Yangjiakuang gold deposit, yielded a Sm-Nd isochron age of 123.5 ± 8.1 Ma (MSWD = 0.042). Subsequent geologic events were recorded by quartz diorite porphyrite dyke which are dated at 122.75 ± 0.66 Ma (MSWD = 1.5) by zircon LA-ICP-MS U-Pb dating. It is suggested that the gold mineralization took place in the early period of Early Cretaceous. The *in situ* $\delta^{34}S$ values of pyrites from two stages have a narrow range from + 5.65 to + 9.63‰ with an average value of 8.14‰, which indicate that the source of $\delta^{34}S$ is related to the Guojialing granite and the Fenzishan Group. The lead isotopic compositions of pyrites ($^{206}Pb/^{204}Pb$ = 16.615 to 16.832; $^{207}Pb/^{204}Pb$ = 15.275 to 15.403; $^{208}Pb/^{204}Pb$ = 36.829–37.470) show a consistent origin of the lower crust. The measured $^{3}He/^{4}He$ ($^{40}Ar/^{36}Ar$) of hydrothermal fluids in pyrites are 0.641–1.132 Ra (637.5–1162.7), indicating that the ore-forming fluid originating from a mixing of crustal and mantle components. It is suggested that the gold mineralization is associated with extensional tectonic inversion caused by the rollback of the subducting Izanagi Plate during the early Cretaceous, which triggered partial melting of mantle and lower crust, and subsequent magma mixing and exsolution of ore-bearing fluids. These fluids extracted ore-forming materials from the enclosing rocks of the Jiaodong Group, the Fenzishan Group, and the Guojialing granite to form the ore-forming fluids.

KEYWORDS

S-He-Ar-Pb isotopes, Sm-Nd isochron age, LA-ICP-MS zircon U-Pb dating, Yangjiakuang gold deposit, Jiaodong peninsula

1 Introduction

The Jiaodong Peninsula is located in the southeastern North China Craton (NCC) and hosts world-class gold deposits with total proven reserves of more than 5,000 t of gold (Song et al., 2021; Tian et al., 2022). In the Jiaodong Peninsula, three major gold metallogenic belts have been identified, including the Zhaoyuan-Laizhou Gold Belt, the Penglai-Qixia-Fushan Gold Belt, and the Muping-Rushan Gold Belt (Deng et al., 2020a; Wu et al., 2021). Three types of gold deposits have been identified so far, i.e., the auriferous quartz vein type, the altered rock type, and the interstratified breccia type (Mao et al., 2008; Yang et al., 2014a). Based on the evidence from geological, geochronological, geochemical, and isotope geochemical, previous researcher have been proposed various models for the genesis of three types of gold deposits (Yang and Zhou, 2001; Zhai et al., 2004; Li et al., 2006; Mao et al., 2008; Deng et al., 2011; Zhai and Santosh, 2013; Li et al., 2017; Li and Santosh, 2017; Yuan et al., 2019; Xu Y. et al., 2022; Tian et al., 2022). More recently, several gold deposits of altered rock types (e.g., Yangjiakuang, Dujiaya) (Figure 1B) have been identified in the Penglai-Qixia-Fushan Gold Belt (Ding et al., 2015). The host rocks for these deposits are Paleoproterozoic metamorphic rocks, which are different from the previous altered rock type for the gold deposits whose gold-bearing host rocks are Archean gneiss and Mesozoic granite. However, these deposits have not drawn much attention in the past, and whether the gold deposits distributed along the Penglai-Qixia-Fushan Gold Belt belong to a new episodic gold mineralization is poorly understood. A study on the genesis and geochronology of the Yangjiakuang gold deposit can expand our knowledge regarding the metallogenic theory concerning the Jiaodong gold deposit and provide a theoretical basis for the prospecting of the same type of gold deposit in the area. In this study, the isotopic compositions of sulfur, lead and He-Ar isotopes of the fluid inclusions were used to decipher the source of the fluids responsible for the Yangjiakuang gold mineralization. Calcite Sm-Nd isotopic dating and zircon U-Pb dating for post-mineralized quartz diorite porphyritic dyke were also conducted to constrain the metallogenic age for the Yangjiakuang gold deposit.

2 Geological background

2.1 Regional geology

The Jiaodong Peninsula consists of two major terranes, namely, the Jiaobei terrane to the northwest and the Sulu ultrahigh-pressure (UHP) terrane to the southeast. These terranes are split by the Wulian-Yantai Fault (Deng et al., 2006; 2018; Yang et al., 2014b; Song et al., 2015; Li et al., 2021). The Jiaobei terrain can be further divided into the Jiaobei Uplift in the north and the Jiaolai Basin in the south (Figure 1A) (Deng et al., 2015).

The Jiaodong Peninsula is composed primarily of the Precambrian basement and Mesozoic igneous rocks. The former includes the Archean tonalite-throndhjemite-granodiorite (TTG) gneisses with small amounts of the Jiaodong Group comprising metamorphic supracrustal rocks and mafic granulite/amphibolite lenses, the Paleoproterozoic Fenzishan and Jingshan Groups, and the Neoproterozoic Penglai Group that consist of metasedimentary rocks (Tang et al., 2007; Yang et al., 2014b; Hao et al., 2020). Geochronological and geochemical studies have revealed that the TTG gneiss, amphibolite, and granulite have protolith ages of ~2.9 to 2.7 Ga, 2.5 Ga, and 2.4 Ga, respectively (Jahn et al., 2008; Xie et al., 2014; Liu et al., 2015; Xie et al., 2015; Dang et al., 2022). The Jingshan Group which is composed of biotite granulite, garnet-biotite-graphite gneiss, dolomitic marble, diopside amphibolite, marble, and biotite-graphite schist (An, 1990; Li et al., 2018; Liu. Z. K et al., 2021), were metamorphosed at 1.8–1.7 Ga under amphibolite to granulite facies (Zhao and Zhai, 2013). The coeval Fenzishan Group has similar source rocks and lithologic compositions to those of the Jingshan Group, whereas the metamorphic grade is low, ranging from greenschist to lower amphibolite facies (Wang et al., 2009; Tan et al., 2015). Subsequently, the Neoproterozoic Penglai Group, which consists of fluvial-clastic and carbonate rocks, underwent lower greenschist-facies metamorphism to form slate, quartzite, and limestone (Faure et al., 2003; Zhang et al., 2010; Tan et al., 2015; Liu. Z. K et al., 2021). This Precambrian basement is partly overlain by Cretaceous continental sediments and volcanic associations emplaced in the Jiaolai Basin (Liu. Z. K et al., 2021).

During the Mesozoic, extensive magmatism took place and formed a series of granitoids and mafic dykes. These processes can be divided into four magma activities based on detailed U-Pb dating: 1) The late Triassic post-collisional rocks (230–200 Ma, Chen et al., 2003; Yang et al., 2005; Guo et al., 2005; Zhang. L et al., 2020) consisting of quartz syenite, pyroxene syenite, and alkaline gabbro, distributed in the Sulu orogenic belt and represented by Shidao, Ningjinsuo, and Chashan intrusions. 2) The late Jurassic calc-alkaline granites (160–141 Ma, Yang et al., 2012; Ma et al., 2013; Li et al., 2019; Wang et al., 2022), which occur as a large batholith and are composed of biotite monzogranite, monzodiorite, quartz diorite, and granodiorite, such as Linglong, Kunyushan, Queshan and Wendeng plutons. 3) The early stage of the Early Cretaceous high-potassium calc-alkaline granodiorite (132–123 Ma, Wang et al., 2014; Liu et al., 2014; Zhao et al., 2018). They are probable mixed crust-mantle components and are represented by the Sanshandao, Shangzhuang, Beijie, Congjia, and Guojialing intrusions (Dang et al., 2022). 4) The late period of the Early Cretaceous alkaline granites and intermediate basic dykes (118–108 Ma, Qiu et al., 2008; Ding et al., 2013; Zhao et al., 2018; Li et al., 2019; Song et al., 2020), which are composed of diorite, granodiorite, and granite assemblages (Yang et al., 2014a; Ding et al., 2015; Dang et al., 2022).

The dominant structures in the Jiaodong Peninsula are NNE-to NE-trending fault systems (Figure 1B). These faults are characterized by a parallel and uniform distribution. From west to east, they are represented by the Sanshandao, Jiaojia, Zhaoping, Qixia, Muping-Jimo, and Jinniushan faults. These structures control the distribution of the Jiaodong gold deposits, which are divided into three gold belts according to their spatial distribution and traditionally have been grouped into three main types (Figure 1B): the auriferous quartz vein type (Linglong type), the altered rock type (Jiaojia type), and the interstratified breccia type (Pengjiakuang type) (Zhang et al., 2003; Mao et al., 2008; Guo et al., 2013). The Linglong type deposits are represented by deposits at Linglong, Denggezhuang, Dayingezhuang, and Jinqingding, whereas the Jiaojia type deposits are exemplified by deposits at Sanshandao, Jiaojia, Xincheng, Xiadian, and Dayingezhuang. The Pengjiakuang type deposits include those at Pengjiakuang and Dazhuangzi.

In recent years, several gold deposits or outcrops have been discovered in the Penglai-Qixia-Fushan Gold Belt, which are represented by the Yangjiakuang and Dujiaya gold deposits. Although these deposits have a similar fault-controlled nature of

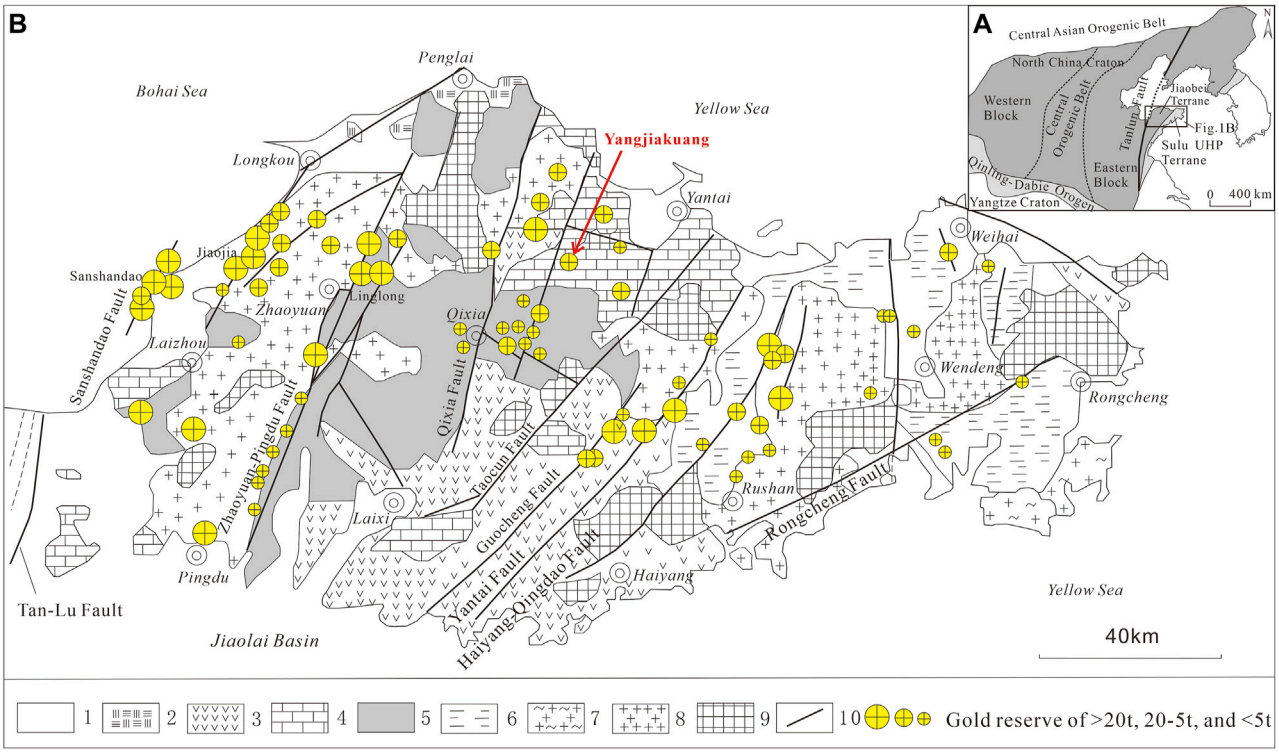

FIGURE 1
Simplified geological map of the Jiaodong Peninsula, showing the distribution of gold deposits, strata, magmatic rocks, and main faults **(B)**. Inset shows tectonic blocks of the North China Craton and the location of the Jiaodong Peninsula **(A)** (simplified from Ding et al., 2015; Li et al., 2020; Dang et al., 2022). 1. Cenozoic sedimentary rocks; 2. Cenozoic basalts; 3. Cretaceous volcanic rocks; 4. Paleoproterozoic Jingshan Group and Fenzishan Group metamorphic rocks; 5. Neoarchean TTG and metamorphic supracrustal rocks; 6. Proterozoic granitic complex rocks; 7. Triassic granites; 8. Jurassic granites; 9. Cretaceous granites; 10. Regional faults.

the mineralization when compared to the traditional three types of Jiaodong deposits, they are characterized by the fact that the gold deposits are hosted in the Paleoproterozoic Fenzishan Group which consist of metamorphic rocks. The detailed geology, mineralization, and alterations are summarized below.

2.2 Deposit geology

The Yangjiakuang gold deposit is located in the Qixia-Penglai-Fushan Gold Belt and belongs to the Jiaobei uplift in the Northeastern margin of the North China Craton (Li et al., 2005; Ding et al., 2015; Song et al., 2015) (Figure 1B). The area mainly exposes thick dolomite marble with biotite granulite, tremolite schist, and tremolite marble in the Paleoproterozoic Zhanggezhuang Formation of the Fenzishan Group, followed by thin-layer calcareous slate, siliceous slate, phyletic slate, and dolomite marble in the Neoproterozoic Baoshankou Formation of the Penglai Group. Mesozoic dykes are developed in the area, including quartz diorite porphyrite, lamprophyre, and pegmatite. All of them are filled with irregular veins and lenticular faults in different directions.

The structure in the area is dominated by a syncline. Mineralization is structurally controlled by the Yangjiakuang syncline in this area. The axis of the syncline, distributed in an EW direction, is located in the west of the Yangjiakuang village (Figure 1). The stratum of the axis consists of the third member of the Zhanggezhuang Formation in the Fenzishan Group, and the two wings consist of the second member, and the first member of the Zhanggezhuang Formation (Figure 2). The strata of the wings present as a reverse sequence. The Western end of the syncline is cut by NNE trending faults, and the eastern end of the syncline dips. The faults are divided into NNE and EW groups. The shape and scale of the Yangjiakuang gold deposit are controlled by the Yangjiakuang syncline. The gold ore body occurs mainly in the marble of the Paleoproterozoic Fenzishan Group, and it is controlled by the interlayer detachment structure and the NE trending fault (Zhang et al., 2004).

Both No. III and No. IV gold orebodies that were explored in the Yangjiakuang deposit are controlled by the Yangjiakuang syncline (Yu et al., 2014). The shape of gold orebody is V-shaped (Figure 2). No. III gold orebody is located in dolomite marble of the third member of Zhanggezhuang Formation near the axis of the structure of Yangjiakuang syncline and has a length of about 950 m and a width of 10–70 m. No. IV gold orebody is hosted in the contact zone between the second and third members of the Zhanggezhuang Formation and has a length of 850 m and a width of 5–16 m (Figure 3), whose proven gold resource is 1.02 t. No. III gold orebody is the largest in the Yangjiakuang deposit and strikes EW, dips to the north at 20–30°, and has a length of 300 m, and a thickness of 4.2–18.0 m. The gold proven resource is 2.58 t. The grade of gold varies from 2.5 to 4.5 g/t, with an average value of 3.79 g/t. The boundary between the orebody and the ore-bearing rock is not clear and shows a gradual

10.3389/feart.2023.1048509

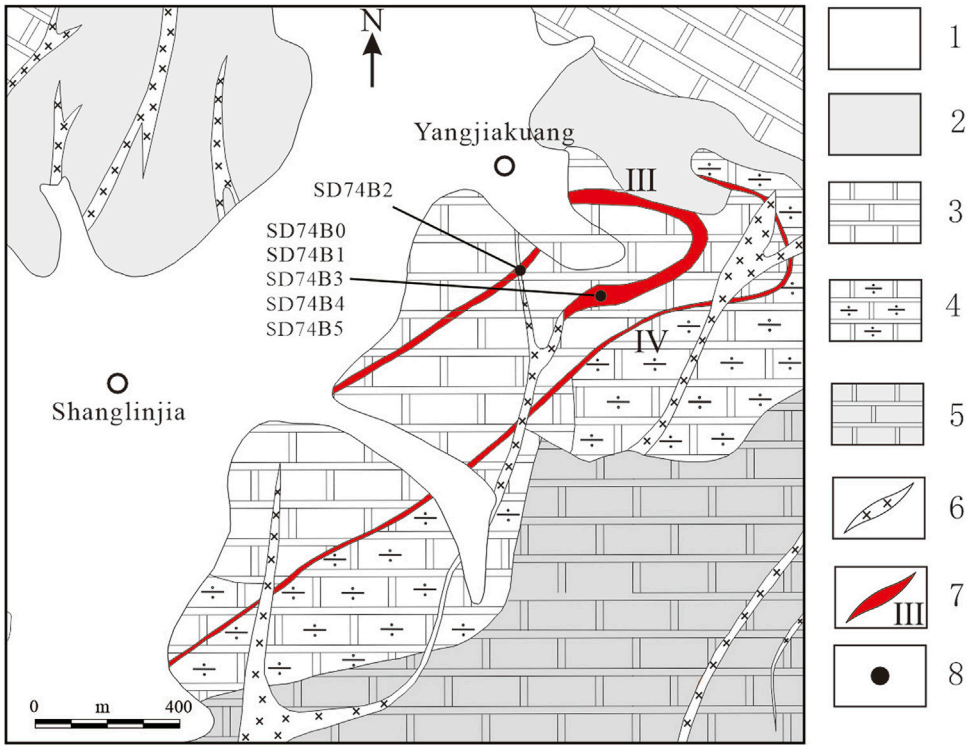

FIGURE 2
Geological sketch map of the Yangjiakuang gold deposit (after Ding, 2014). 1. Quaternary; 2. Slate (Baoshankou Formation); 3. Dolomite marble (Third member of the Zhanggezhuang Formation); 4. Diorite marble (Second member of the Zhanggezhuang Formation); 5. Dolomite marble (First member of the Zhanggezhuang Formation); 6. Quartz diorite porphyrite; 7. Gold orebody; 8. Sample location.

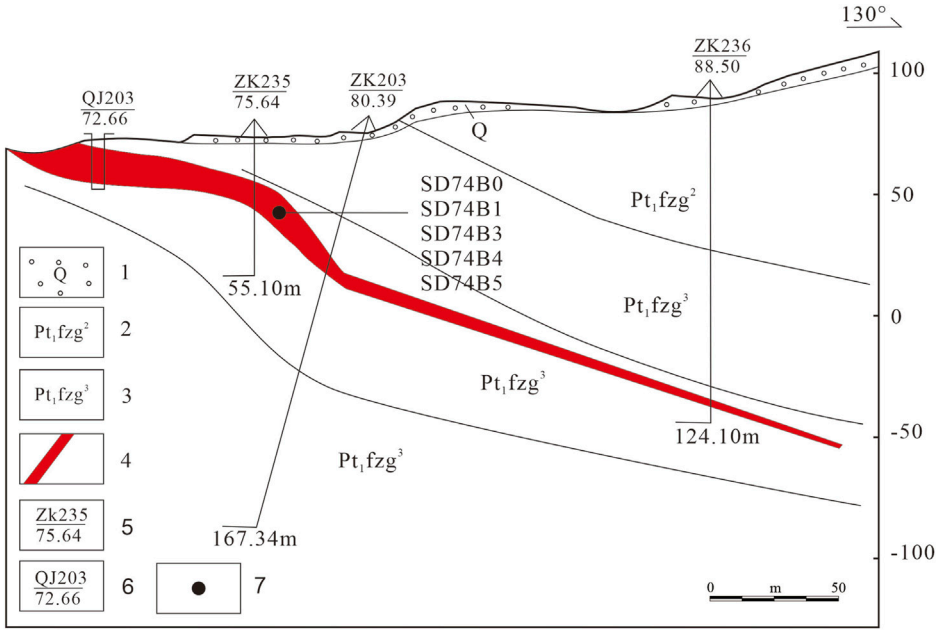

FIGURE 3
Geological profile along No. 252 line of the Yangjiakuang gold deposit, showing the sampling sites in this study (after Yu et al., 2014). 1. Quaternary; 2. Second member of the Zhanggezhuang Formation; 3. Third member of the Zhanggezhuang Formation; 4. Gold vein; 5. Drill hole; 6. Drilling shallow well; 7. Sample location.

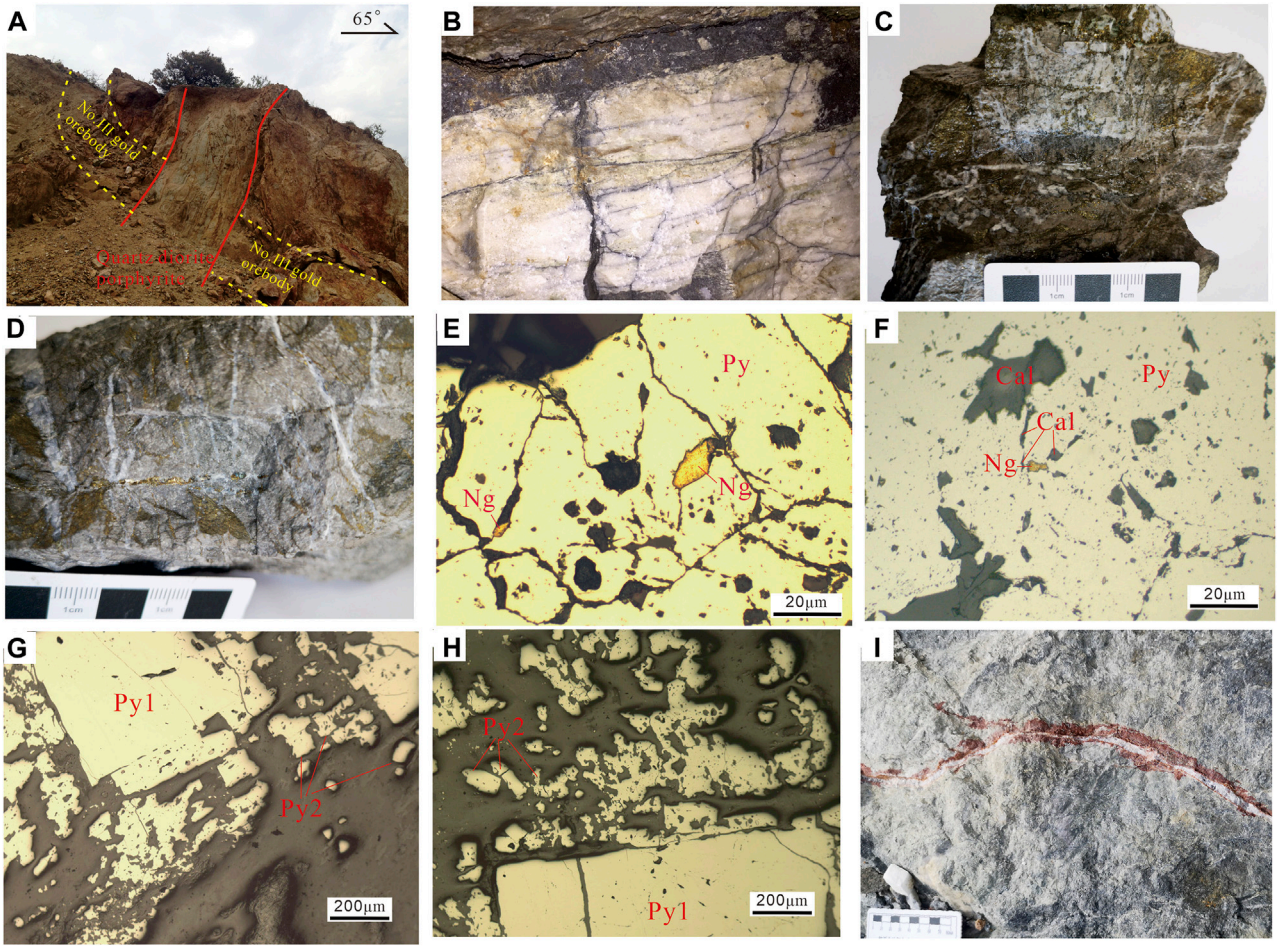

FIGURE 4
Photographs showing mineral assemblages and mineralization stages in the Yangjiakuang gold deposit **(A)** Quartz diorite porphyrite dyke cutting through the gold orebody; **(B)** Disseminated-type ore; **(C,D)** Veinlet-type ore; **(E,F)** Irregular native gold inclusions within Py; **(G,H)** Micrographs of Py1 and Py2; **(I)** Quartz and calcite vein; Mineral abbreviations used are as follows: Py, Pyrite; Cal, Calcite; Ng, Natural gold.

transitional relationship, which is determined solely by the grade of gold. The ore-bearing rock near the orebody is mainly sericite cataclastic marble, followed by granulite, amphibolite, diorite, slate, *etc.* The quartz diorite porphyry dyke located in the west of Yangjiakuang gold deposit cuts through No. III gold orebody (Figure 4A), which should be close to or later than the gold mineralization. The strike is mostly 0°–10° and dips 75° to East, and measure 5–20 m in width and 750 m in length. The quartz diorite porphyrite is gray and featured a massive porphyritic structure. The phenocrysts were composed of plagioclase and quartz, and the substrate was composed of plagioclase, amphibole, biotite, and quartz. The content of plagioclase was 65%, which was an idiomorphic plate with lamellar twins; the hornblende content was 5%–10% with an idiomorphic plate; the quartz content was about 15%, the phenocryst melting corrosion was round, and the matrix was granular in nature; the K-feldspar content was 10%–15%, appearing in the matrix in the form of lath.

Disseminated- and veinlet-type ores can be observed in the Yangjiakuang gold deposit (Figures 4B–D). Ore minerals are dominated by pyrite with lesser amounts of chalcopyrite, sphalerite, arsenopyrite, and magnetite. The main precious metals are natural gold, silver-bearing natural gold and natural silver. The gangue minerals consist of quartz, calcite, and sericite, with subordinate chlorite, epidote, tremolite, graphite, and barite. The main elements in the ore are Au, followed by Ag. Gold occurs mostly as natural gold and silver-bearing natural gold. The microscopic observations show that the visible gold mainly occurs as filling microfractures in pyrite or as inclusions in pyrite and less commonly in calcite (Figures 4E, F). Native gold grains are generally less than 10 μm.

Three hydrothermal stages can be recognized in the Yangjiakuang gold deposit, on the basis of field evidence and microscopic texture, from oldest to youngest they are: the pyrite-sericite stage (I), the gold, polymetallic sulfide, and quartz stage (II), and quartz-calcite Stage (III). Stage I is represented by an assemblage of quartz, sericite and pyrite. The pyrite of this stage is euhedral, with 3–10 μm in size and essentially barren of gold (Figures 4G, H). The quartz is milky white and fine-grained. The sericite is distributed in fine grain orientation. Stage II is characterized by gold-bearing fine pyrite, quartz, and a small amount of chalcopyrite, sphalerite, galena, and calcite. A large amount of gold-bearing pyrites are formed in this stage (Figures 4G, H), which represents the main gold mineralization stage. Stage III is dominated by carbonate minerals (mainly calcite) and quartz (Figure 4I). They

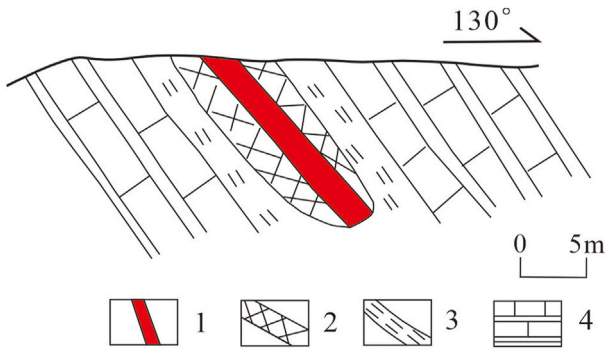

FIGURE 5
Diagram of wall-rock alteration zone for the Yangjiakuang gold deposit. 1. Gold vein; 2. Auriferous pyrite-quartz vein; 3. Sericitization zone; 4. Carbonation zone.

often occur as micro-to macroscopic veinlet-shaped forms. This is the latest mineralization stage.

Hydrothermal alteration is widespread, including sericitization, silicification, pyritization, carbonation, chloritization, and tremolite. The silicification, pyritization, and sericitization are closely related to gold mineralization (Wang et al., 2017). There is a gradual transitional relationship between the gold orebody and the surrounding rocks (Figure 5). The core of the gold orebody is mainly composed of quartz, sericite, and pyrite. The sericite is distributed in a scale-like orientation, quartz is arranged in an allomorphic granular orientation, and pyrite occurs in a veined and disseminated form. The wall rock near the orebody is composed of quartz, sericite, and a small amount of calcite, which developed silicification and sericitization alteration. In the wall rock distant to the orebody, the mineral compositions are mainly protolith, and quartz and calcite veinlets which formed by the late alteration and filled along the fractures.

3 Analytical methods

Except for the quartz diorite porphyry dyke which was mined in the shallow surface, all of the samples were mined underground in tunnels of depth 60 m.

In situ S isotope analyses of five samples from different stage sulfides in thin sections were performed by LA-MC-ICP-MS at the State Key Laboratory of Geological Processes and Mineral Resources, China University of Geosciences (Wuhan). The analytical methods are based on Bendall et al. (2006) and Craddock et al. (2008). A Nu Plasma II MC-ICP-MS equipped with a Resolution-S155 excimer ArF laser ablation system was used for the analyses. The detailed experimental procedures and instrument test parameters were conducted according to Liu et al. (2018), Tian et al. (2020) and Xu Y. W. et al (2022).

He-Ar isotope analyses were performed at the Analytical and Testing Center in the Beijing Institute of Geological Research of Nuclear Industry, Beijing. The Helix SFT™ Split Flight Tube noble gas mass spectrometer was used, which had blank background signals of less than 5×10^{-14} ccSTP, a Faraday cup resolution greater than 400, and an ion multiplier resolution better than 700. The sensitivity of the He and Ar measurements were better than 2×10^{-4} A/Torr and 1×10^{-3}A/Torr, respectively. Four samples corresponding to stage II were measured. The analytical procedures adopted were the same as those described by Wang (2016), Tian et al. (2020) and Xu Y. et al (2022).

Lead isotope analyses were performed by a thermal ionization mass spectrometer (ISOPROBE-T) at the Beijing Institute of Geological Research of Nuclear Industry. The measured Pb isotopic ratio measurements for the international standard NBS 981 are around 0.1‰. The analytical values for the standard NBS 981 were as follows: $^{206}Pb/^{204}Pb = 16.937 \pm 0.002$ (2σ), $^{207}Pb/^{204}Pb = 15.457 \pm 0.002$ (2σ), and $^{208}Pb/^{204}Pb = 272\ 36.611 \pm 0.004$ (2σ) (Tian et al., 2020).

In order to constrain the timing of the main mineralization, eight calcites were collected for Sm-Nd dating. The calcite of the Yangjiakuang gold deposit was milky white and veinlet, coexisting with disseminated pyrite and other gold-bearing minerals. The aforementioned samples were collected and pulverized in the field to 40–60 mesh, and calcite was selected with the aid of a binocular lens, The sample, of purity better than 99%, was rinsed with distilled water, steam dried at low temperature, and then ground to about 200 mesh in the agate mortar prior to testing. Analyses of the Sm-Nd isotopes were carried out at the Isotope Geochronology Laboratory of the Tianjin Center, China Geological Survey. A description of the separation processes including the use of a specific resin are given elsewhere (Liu et al., 2017; Liu et al., 2018; Li et al., 2020), and the isochron age was calculated by the ISOPLOT program.

The U-Pb isotopic dating of zircon by LA-ICP-MS was undertaken in the laboratory of isotopic geochronology of the Tianjin Center, China Geological Survey. First, Zircons were separated from the quartz diorite porphyry dyke (SD74B2) using conventional crushing and sieving followed by standard heavy liquid and magnetic separation before pure separates were obtained by hand-picking under a binocular microscope at the Hebei Institute of Regional Geological and Mineral Resource Survey (Langfang). The separated zircons were then mounted in epoxy and polished to expose grain center for optical microscopy and cathodoluminescence (CL) imaging to identify target areas for U-Pb analyses (Figure 6).

Zircon LA-ICP-MS U-Pb analysis was undertaken in the laboratory of isotopic geochronology of the Tianjin Center, China Geological Survey. This analysis used laser energy and frequency settings of 13–14 J/cm^2 and 9 Hz, respectively, with a spot size of 35 μm. Helium was used as a carrier gas, and each analysis incorporated a background acquisition of ~20 s (gas blank), followed by 40 s of acquisition (ablated sample). GJ-1 was used as the external standard for the zircon age with correction for fractionation in the U-Pb isotope measurement (Jackson et al., 2004). The DataCal program for ICP-MS developed by Liu et al. (2010) and the Isoplot program developed by Ludwig (2003) were used for data processing. The isotopic data for the common lead was corrected by the ^{208}Pb correction method (Andersen, 2002). The Pb, U, and Th contents of the zircon samples were calculated based on using the NIST 610 glass standard as an external standard. Please consult Li et al. (2009) for full information on the instrument operating procedures and conditions.

4 Results

4.1 *In situ* sulfur isotopes

In situ measurements of sulfur isotopes at 18 locations on pyrite were conducted and the results are presented in Table 1. The pyrite

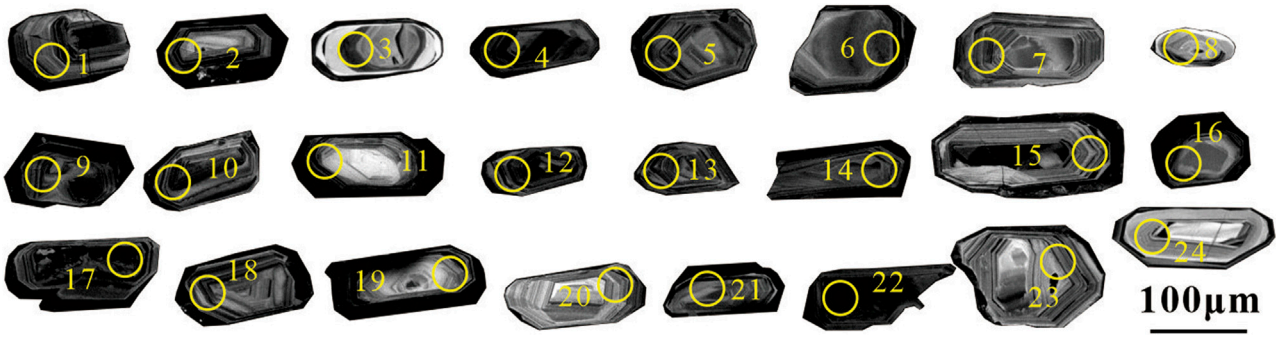

FIGURE 6
CL images and U-Pb data of zircons in diorite porphyrite (SD74B2).

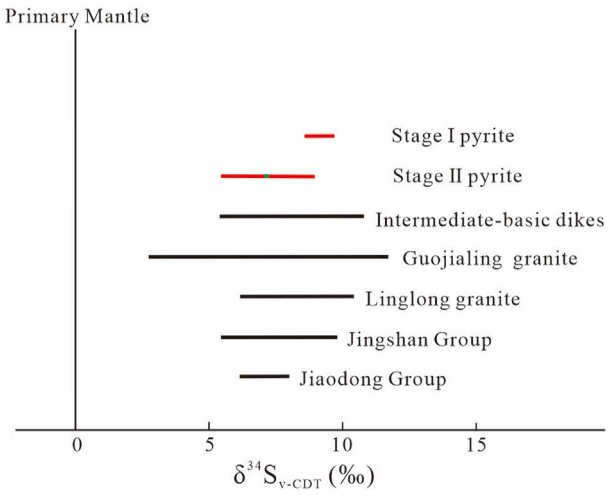

FIGURE 7
Sulfur isotopic compositions of pyrites from the Yangjiakuang gold deposit. The ranges of major geologic units are from Tian et al., 2020; Li et al., 2021; Liu. X. Y et al., 2021.

$\delta^{34}S$ values were distributed in a narrow range of 5.65–9.63‰, with an average value of 8.14‰. Pyrite $\delta^{34}S$ values (n = 6) for Stage I were 8.5–9.6‰ (avg. 9.1‰) and pyrite $\delta^{34}S$ values (n = 12) for stage II were 5.6–8.9‰ (avg. 7.6‰) (Figure 7).

The pyrite $\delta^{34}S$ values for the Yangjiakuang deposit were positive in different hydrothermal stages (9.1‰ for stage I→7.6‰ for stage II), which are similar to those of other Jiaodong gold deposits (e.g., Linglong deposit = 5.6–7.9‰, Guo et al., 2020; Dayingezhuang deposit = 4.8–9.0‰, Yuan et al., 2019; Heilangou deposit = 5.5–7.8‰; Xincheng deposit = 7.2–9.7‰, Majiayao deposit = 6.0–10.7‰, Tian et al., 2020 and Zhaoxian deposit = 6.0–10.7‰, Xu et al., 2022). These results indicate that the source of sulfur for the Yangjiakuang gold deposit was similar to the other neighboring gold deposits.

4.2 Helium-argon isotopes

The Helium and argon isotopic compositions of pyrites from different mineralization stages are shown in Table 2. The ^{3}He values for the fluid inclusions in pyrites ranged from 3.587 to 5.016×10^{-13} cm^3 STP/g, with an average value of 4.516×10^{-13} cm^3STP/g; the ^{4}He values ranged from 31.61 to 78.63×10^{-8} cm^3STP/g, with an average value of 53.95×10^{-8} cm^3STP/g. The $^{3}He/^{4}He$ ratios ranged from 0.641 to 1.132 Ra, with an average value of 0.901 Ra (Table 2). In the evolution diagram for the ^{3}He-^{4}He isotopes, the Helium and Argon isotopic values are projected in the crust and mantle transition field (Figure 8). In the diagram of Rc/Ra-$^{40}Ar/^{36}Ar$, the Helium and Argon isotopic values are also projected in the crust and mantle transition field which is near the meteoric water (Figure 9). The results show that the ore-forming fluids represent a mixture of crust and mantle fluids, and litter meteoric water.

4.3 Lead isotopes

The lead isotope ratios for seven pyrites were measured and the results are presented in Table 3. The values for $^{206}Pb/^{204}Pb$, $^{207}Pb/^{204}Pb$, and $^{208}Pb/^{204}Pb$ ranged from 16.615 to 16.832, 15.275 to 15.403, and 36.829 to 37.470, respectively. All the lead isotope values plotted in the field correspond to a lower crustal origin as per the diagram of lead isotope tectonic environments created by Zartman and Doe (1981) (Figure 10).

LC, lower crust; UC, upper crust; OIV, ocean island volcanic; OR, orogenic belts.

The region of Pb isotopes for the Jiaodong sulfide or ore is determined by Liu. Z. K et al., 2021.

4.4 Calcite Sm-Nd age

The Sm-Nd isotopic dating for eight calcites were measured and the results are shown in Table 4.

The mass fractions for Sm and Nd of calcites ranged from 1.23 to 4.73×10^{-6} and 5.90 to 17.18×10^{-6} with $^{147}Sm/^{144}Nd$ and $^{143}Nd/^{144}Nd$ values ranging from 0.1045 to 0.1664 and 0.511135 to 0.511185, respectively. The $^{147}Sm/^{144}Nd$ and $^{143}Nd/^{144}Nd$ values for calcites exhibited a good linear relationship. An isochronous age of 123.5 ± 8.1 Ma (MSWD = 0.042) and an initial $^{143}Nd/^{144}Nd$ value of 0.5110504 for calcites were obtained (Figure 11). It represents that the Yangjiakuang gold mineralization is the early period of Early Cretaceous.

10.3389/feart.2023.1048509

TABLE 1 LA-MC-ICP-MS *in situ* S isotopic compositions of different hydrothermal stages of pyrites from the Yangjiakuang gold deposit.

Stage	Sample serial number	Mineral	$\delta^{34}S_{CDT}$ (‰)	Source
Stage Ⅰ	SD74B0-1	Pyrite	8.7	This study
	SD74B0-2	Pyrite	9.6	
	SD74B0-3	Pyrite	9.6	
	SD74B0-1	Pyrite	8.5	
	SD74B0-2	Pyrite	9.1	
	SD74B0-3	Pyrite	9.3	
Stage Ⅱ	SD74B1-1	Pyrite	8.6	This study
	SD74B1-2	Pyrite	8.9	
	SD74B1-3	Pyrite	7.1	
	SD74B1-4	Pyrite	5.6	
	SD74B3-1	Pyrite	7.1	
	SD74B3-2	Pyrite	7.8	
	SD74B4-1	Pyrite	7.3	
	SD74B4-2	Pyrite	8.3	
	SD74B4-3	Pyrite	6.5	
	SD74B5-1	Pyrite	8.2	
	SD74B5-2	Pyrite	7.1	
	SD74B5-3	Pyrite	8.5	

TABLE 2 He and Ar isotopic compositions of fluid inclusions in pyrites from the Yangjiakuang gold deposit.

Sample No.	$^{40}Ar/^{36}Ar$	Standard Error	$^{36}Ar/^{38}Ar$	Standard Error	$^{3}He/^{4}He$ (10^{-7})	Standard Error	Content (cm^3STP/g)		
							^{40}Ar (10^{-8})	^{4}He (10^{-8})	^{3}He (10^{-13})
SD74B 1-1	637.5	0.93	5.31	0.04	6.41	0.45	53.71	78.63	5.052
SD74B 1-2	1162.7	1.39	5.29	0.01	7.32	0.89	49.52	60.12	4.411
SD74B 3-1	960.8	1.25	5.36	0.03	11.01	1.07	21.11	45.43	5.016
SD74B4-1	981.5	3.78	5.33	0.05	11.32	1.28	47.59	31.61	3.587

Notes: Rc is the.^{3}He/4He value of samples, Ra is the ^{3}He/^{4}He of the atmosphere (1.40×10^{-6}). The He isotopes were measured at the Mineral Resources Research Institute, Chinese Academy of Geological Sciences.

TABLE 3 Lead isotopic compositions of pyrites from the Yangjiakuang gold deposit.

Sample No.	Mineral	$^{206}Pb/^{204}Pb$	$^{207}Pb/^{204}Pb$	$^{208}Pb/^{204}Pb$	References
SD74B1-1	Pyrite	16.832	15.403	37.470	This study
SD74B1-2	Pyrite	16.803	15.401	37.352	
SD74B3-1	Pyrite	16.795	15.383	37.298	
SD74B3-3	Pyrite	16.812	15.379	37.295	
SD74B4-2	Pyrite	16.814	15.386	37.320	
SD74B4-3	Pyrite	16.615	15.275	36.829	
SD74B5-1	Pyrite	16.715	15.312	37.128	

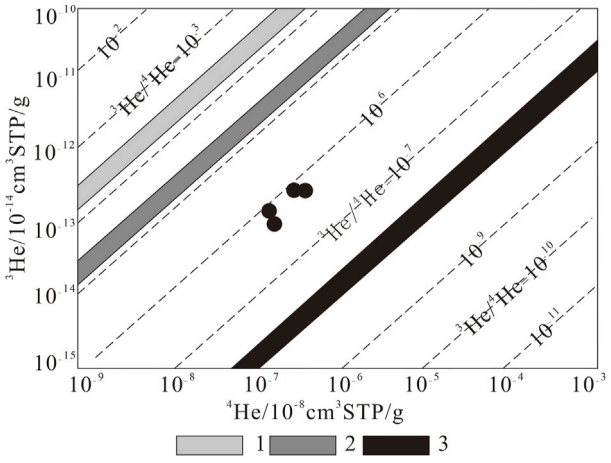

FIGURE 8
Helium isotopic compositions of fluid inclusions in pyrites from the Yangjiakuang gold deposit (after Mamyrin & Tolstikhin, 1984). 1. Initial argon; 2. Mantle argon; 3. Crustal argon.

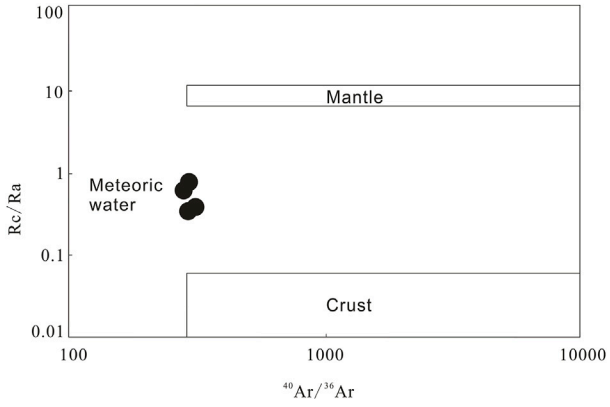

FIGURE 9
Plot of Rc/Ra–^{40}Ar/^{36}Ar ratios of fluid inclusions in pyrites from the Yangjiakuang gold deposit.

4.5 Zircon U-Pb dating

Zircons from the quartz diorite porphyrite dyke (SD74B2) in the Yangjiakuang gold deposit were mostly short columns, with high transparency, euhedral or subhedral, about 60 μm–90 μm in length. The zircons had a typical magmatic concussion zone. Representative CL images are shown in Figure 6. The U content for the zircons ranged from 289 × 10^{-6} ~ 1603 × 10^{-5} and the Th content was from 36 × 10^{-7} ~ 579 × 10^{-6}. The Th/U ratios ranged from 0.12 to 0.73 and the average value was 0.26 (Table 5; Figure 12). The results for the ages of 24 analysis points were relatively concentrated and they could be classified into three groups. The first group was the magmatic zircon age consisting of 21 analysis results. This age was concentrated on the consistent curve on the harmonic map of Figure 11. The range for the ^{206}Pb/^{238}U age was 126–121 Ma, and the weighted average age was 122.75 ± 0.66 Ma (MSWD = 1.5) (Figure 12), which represents the emplacement age of the quartz diorite porphyrite dyke. The second group was the inherited zircon age, which consisted of three analysis results. The ^{206}Pb/^{238}U ages for sample No. 3 and sample No. 8 were 2472 Ma and 2490 Ma, respectively. It is speculated that these ages represent the inherited zircon ages of ancient gneiss in the Jiaodong area. The third group has only one inherited zircon age (sample No. 24), the apparent age being 151 Ma, which may reflect the inherited zircon age of Linglong granite.

5 Discussion

5.1 Mineralization age

Based on various isotopic dating methods (e.g., hydrothermal zircon U-Pb dating, hydrothermal monazite U-Pb dating, mineralization related muscovite Ar-Ar dating), decades of geochronological research on large-scale gold mineralization in the Jiaodong Peninsula indicate an episode of gold mineralization was 130–120 Ma (Luo and Miao, 2002; Zhai et al., 2004; Chen et al., 2005; Fan et al., 2005; Li et al., 2005; Li et al., 2008; Yang et al., 2014b; Zhu et al., 2015; Li and Santosh, 2017; Deng et al., 2020b, 2020c; Zhang. H. Y et al., 2020). Li et al. (2020) proposed that there were two large-scale gold mineralization events, including the early period of Early Cretaceous (126–120 Ma), which formed the Laizhou-Zhaoyuan and Qixia-Penglai-Fushan Gold Belts in the north-west of Jiaodong terrane, and the late period of Early Cretaceous (110–104 Ma), forming the Muping-Rushan Gold Belt in the north-east of the Jiaodong terrane (Li et al., 2020).

Recent studies have shown that strong fractionation between rare Earth elements can occur during the formation of hydrothermal deposits, leading to large changes in Sm and Nd contents in some hydrothermal minerals, reaching values far higher than the normal values of crustal rocks. This discovery lays a foundation for the application of Sm-Nd isotopes in metallogenic chronology (Zhao & Jiang, 2004). Calcium-bearing minerals are always rich in rare Earth elements, making fluorite, calcite, and other calcium-bearing minerals to be the ideal targets for Sm-Nd isotopic dating of hydrothermal deposits (Bell et al., 1989; Jiang et al., 2000; Brugger et al., 2002; Li et al., 2006; Jahn et al., 2008; Peng et al., 2008; Li et al., 2020). The calcite is the main mineral formed during the metallizing stage in the Yangjiakuang and Tudui gold deposits, and contains natural gold in the calcite quartz veinlets (Ding et al., 2015; Zhang, 2018). Therefore, the calcite can represent the age of main gold mineralization. This paper yields calcite Sm-Nd isochron age as 123.5 ± 8.1 Ma, which represents the main gold metallogenic stage (II) at Yangjiakuang gold deposit.

LA-ICP-MS zircon U-Pb dating for quartz diorite porphyrite dyke is 122.75 ± 0.66 Ma, which represents the post-mineralization age. In summary, the mineralization of Yangjiakuang gold deposit is the early period of Early Cretaceous, and it is consistent with the first large-scale gold mineralization in Jiaodong Peninsula.

5.2 Source of the ore-forming materials and fluids

The δ^{34}S values of sulfides from the Yangjiakuang gold deposit vary from 5.65 to 9.63‰, with an average value of 8.14‰. This narrow range of sulfur isotope compositions suggests that the physicochemical

TABLE 4 Sm-Nd isotopic compositions of calcites from the Yangjiakuang gold deposit.

Sample No.	Sm (× 10^{-6})	Nd (× 10^{-6})	$^{147}Sm/^{144}Nd$	$^{143}Nd/^{144}Nd$	2σ
SD74B1-1	3.42	12.70	0.1628	0.511182	0.0009
SD74B1-2	2.56	10.63	0.1456	0.511168	0.0006
SD74B1-3	2.57	11.71	0.1326	0.511157	0.0005
SD74B1-4	1.72	9.97	0.1045	0.511135	0.0007
SD74B1-5	1.23	5.90	0.1264	0.511153	0.001
SD74B1-6	4.73	17.18	0.1664	0.511185	0.0005
SD74B1-7	2.52	13.76	0.1107	0.511140	0.0006
SD74B1-8	3.08	12.18	0.1529	0.511174	0.0009

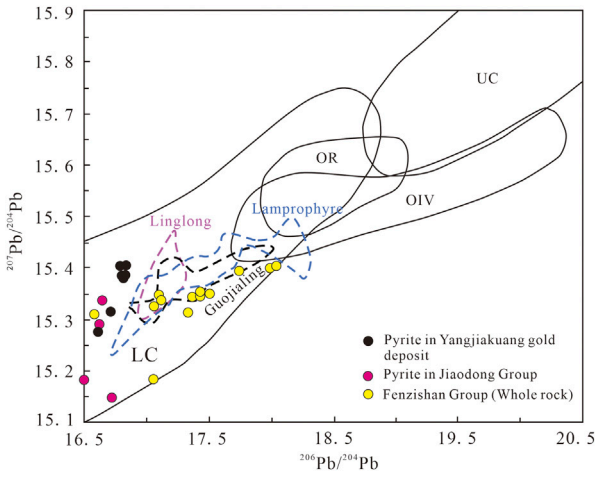

FIGURE 10
$^{206}Pb/^{204}Pb$–$^{207}Pb/^{204}Pb$ diagram of the Yangjiakuang gold deposit (after Zartman & Doe, 1981).

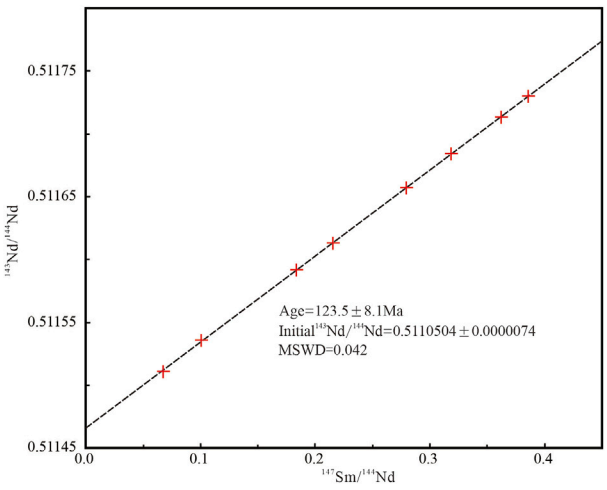

FIGURE 11
Diagram of calcite Sm-Nd isochronous age for the Yangjiakuang gold deposit.

parameters of the mineralizing fluids were relatively constant (Saravanan and Mishra, 2009; Li et al., 2012). In addition, the sulfide assemblage is simple and dominated by pyrite, and thus the $\delta^{34}S$ values of pyrite can be used for tracing the source of ore fluids (Kajiwara and Krouse, 1971; Ohmoto, 1972).

The values of the sulfur isotopes observed are clearly larger than those of magmatic-derived sulfur. Combined with the geologic constraints, at least five sources might account for such sulfur signatures: Precambrian basement, Paleoproterozoic Fenzishan Group, Mesozoic granitoid intrusions, mafic dykes, or multiple sources. Previous studies reported that the sulfur isotopic values of the Fenzishan Group, the Jiaodong Group, the Jurassic-Cretaceous granites, and the Cretaceous dykes were 5.6–12.0‰, 0.0–10.8‰, 2.0–9.9‰, and -3.4–9.9‰, respectively (Figure 7) (Yang et al., 2005; Li et al., 2015; Guo et al., 2017; Deng et al., 2020a). However, the metamorphic devolatization of the Precambrian basement cannot provide sulfur and mineralizing fluids directly, although the Fenzishan Group has similar $\delta^{34}S$ values to the sulfide ores studied (Tan et al., 2015). The apparent time gap (20–40 Ma) between the gold mineralization and the Jurassic granitoids (Linglong granite) (160–150 Ma, Yang et al., 2012; Ma et al., 2013; Li et al., 2019) precludes a hydrothermal link between these two. In addition, the Cretaceous intermediate dyke (118–108 Ma, Qiu et al., 2008; Ding et al., 2013; Zhao et al., 2018; Li et al., 2019; Song et al., 2020), also cannot provide the source of ore-forming sulfur, because of its formation later than that of gold mineralization. The potential candidate for the source of sulfur may be represented by Guojialing granite that intruded intensively in this district. Integrating the values with the aforementioned $\delta^{34}S$ values of the Fenzishan Group, we suggest that there were multi-sources for the sulfur in the ore system *via* magmatic-derived fluids leaching from the Fenzishan Group.

The noble gases have distinct isotopic compositions in the different reservoirs, and the magnitude of the isotopic ratio values can signify the presence of crust and mantle components during the ore-forming processes (Kendrick and Burnard, 2013). Therefore, noble gases can be used as an ideal tracer for the crust and mantle contributions to ore-forming fluids (Turner et al., 1993; Stuart et al., 1995). The $^{3}He/^{4}He$ ratios for the fluid inclusions in pyrite ranged from 0.64 to 1.13 Ra with an average value of 0.90 Ra (Table 2), which is 1–2 orders of magnitude higher than the crustal values (0.01–0.05 Ra, Burnard et al., 1999) but lower than the mantle

10.3389/feart.2023.1048509

TABLE 5 LA-ICP-MS zircon U-Pb data for the quartz diorite porphyrite dyke.

Sample No.	Content (ppm)			Isotopic ratio						Age (Ma)					
	Pb	U	Th/U	$^{206}Pb/^{238}U$	1σ	$^{207}Pb/^{235}U$	1σ	$^{207}Pb/^{206}Pb$	1σ	$^{206}Pb/^{238}U$	1σ	$^{207}Pb/^{235}U$	1σ	$^{207}Pb/^{206}Pb$	1σ
SD74B2-1	12	612	0.31	0.0195	0.0002	0.0485	0.0014	0.0485	0.0014	122	1	122	4	123	68
SD74B2-2	11	562	0.22	0.0199	0.0002	0.0491	0.0016	0.0491	0.0016	125	1	126	4	150	77
SD74B2-3	165	319	0.32	0.4677	0.0048	0.1705	0.0019	0.1705	0.0019	2472	26	2521	33	2560	19
SD74B2-4	16	833	0.24	0.0197	0.0002	0.0485	0.0010	0.0485	0.0010	124	1	124	3	123	48
SD74B2-5	18	983	0.19	0.0191	0.0002	0.0493	0.0018	0.0493	0.0018	120	1	122	5	161	85
SD74B2-6	21	1099	0.28	0.0192	0.0002	0.0505	0.0011	0.0505	0.0011	120	1	125	3	215	53
SD74B2-7	5	289	0.12	0.0199	0.0002	0.0476	0.0026	0.0476	0.0026	125	1	123	7	76	130
SD74B2-8	13	25	0.5	0.4720	0.0107	0.1665	0.0026	0.1665	0.0026	2490	56	2507	69	2521	26
SD74B2-9	20	1072	0.25	0.0192	0.0002	0.0496	0.0010	0.0496	0.0010	121	1	123	3	173	46
SD74B2-10	11	582	0.27	0.0195	0.0002	0.0493	0.0012	0.0493	0.0012	122	1	124	3	160	58
SD74B2-11	18	955	0.17	0.0194	0.0002	0.0495	0.0011	0.0495	0.0011	122	1	124	3	170	52
SD74B2-12	19	1031	0.21	0.0194	0.0002	0.0499	0.0010	0.0499	0.0010	122	1	125	3	190	45
SD74B2-13	14	727	0.21	0.0196	0.0002	0.0489	0.0012	0.0489	0.0012	123	1	124	3	142	57
SD74B2-14	16	829	0.23	0.0198	0.0002	0.0472	0.0010	0.0472	0.0010	124	1	121	3	57	52
SD74B2-15	31	1603	0.25	0.0198	0.0002	0.0481	0.0007	0.0481	0.0007	124	1	123	2	102	35
SD74B2-16	8	417	0.23	0.0197	0.0002	0.0492	0.0021	0.0492	0.0021	124	1	126	6	157	101
SD74B2-17	8	404	0.21	0.0198	0.0002	0.0478	0.0016	0.0478	0.0016	124	1	123	4	90	77
SD74B2-18	21	1119	0.23	0.0193	0.0002	0.0496	0.0009	0.0496	0.0009	121	1	124	2	173	41
SD74B2-19	22	1158	0.21	0.0196	0.0002	0.0486	0.0009	0.0486	0.0009	125	1	123	3	126	45
SD74B2-20	13	689	0.15	0.0199	0.0002	0.0483	0.0013	0.0483	0.0013	125	1	125	4	113	66
SD74B2-21	13	669	0.19	0.0197	0.0002	0.0497	0.0014	0.0497	0.0014	123	1	126	4	1820	67
SD74B2-22	17	930	0.15	0.0198	0.0002	0.0471	0.0009	0.0471	0.0009	124	1	121	3	51	48
SD74B2-23	18	795	0.73	0.0196	0.0002	0.0500	0.0010	0.0500	0.0010	123	1	126	3	192	47
SD74B2-24	10	410	0.29	0.0240	0.0003	0.0493	0.0016	0.0493	0.0016	151	2	151	5	159	76

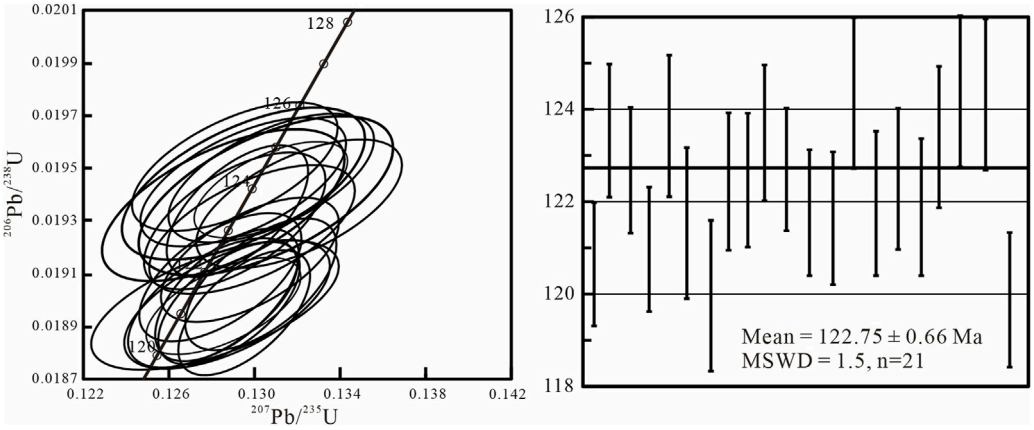

FIGURE 12
Zircon U-Pb Concordia diagram for the quartz diorite porphyrite dyke (SD74B2).

values (6–9 Ra, Stuart et al., 1995), revealing a mixing between the crustal and mantle-derived components in the ore-forming fluids. In the ^{4}He vs. ^{3}He plot, the ^{3}He and ^{4}He isotopic compositions are between the mantle Helium line and the crustal Helium line (Figure 8). In the R/Ra vs. $^{40}Ar/^{36}Ar$ plot (Figure 9), the He and Ar isotopic compositions spread between the mantle field and the crustal field. All these He-Ar isotopic signatures suggest that the ore-forming fluid at Yangjiakuang gold deposit can be regard as a combination of crustal and mantle components.

Lead isotope is a useful indicator for the source of ore-forming materials. The Pb isotopic compositions of pyrites were characterized by a crust-mantle mixing. In the $^{207}Pb/^{204}Pb$ vs. $^{206}Pb/^{204}Pb$ diagram, the pyrites yield a similar lead isotopic compositions and plot in the compositions area of the upper crust (Figure 10). In light of the overlapping field in the Pb isotope diagram (Figure 10), the metamorphic basement of the Jiaodong and Fenzishan Groups, as a member of the lower crust, is suggested as the most likely source of Pb. There is the possibility that the mineralizing fluids selectively leached Pb from the Jiaodong and Fenzishan Groups.

5.3 Geodynamic significance

The age of Yangjiakuang gold mineralization is the early period of Early Cretaceous, which is consistent with the first large-scale gold mineralization in Jiaodong terrane. As it discussed above, the potential candidate for the source of ore-forming materials and fluids may be represented by the Guojialing granites. The S-He-Ar-Pb isotopes suggest that the ore-forming materials of the Yangjiakuang gold deposit may originate from a mixture of crustal and mantle components. The deep crust-mantle derived magma (Guojialing granite) maybe provide the heat sources in the extensional regime for melt and fluid circulation, and then the ore fluid can be separated during the ascent into the upper crust and leached the ore-forming materials from the Fenzishan Group, the Jiaodong Group and the Guojialing granite.

This metallogenic event is widely developed in the Jiaodong gold province. It is suggested that the extensional tectonic inversion event triggering gold mineralization was related to the rollback of the subducting Izanagi plate. Most researchers agree that the Izanagi Plate was subducted beneath northeastern China at ca. 170 Ma (Isozaki, 1997; Maruyama et al., 1997; Zhu et al., 2018). The initial subduction of the plate was rapid and low angle, generating compressive stress in eastern China (Zhang and Zhang., 2007). This low angle subduction meant that the Izanagi Plate was located below northeastern China, thickening and compressing the already thickened orogenic crust formed by earlier continental collisional events, which caused partial melting of the lower crust and lithospheric delamination (Dang et al., 2022). The loss of the lithospheric keel caused the asthenospheric upwelling, lithospheric extension and thinning in the Early Cretaceous. This was associated with the steepening of the angle and the associated rollback of the subducting Izanagi Plate. In an extensional regime, eastern NCC witnessed craton destruction or decratonization (Wu et al., 2005; Yang and Li, 2008; Zhu et al., 2015), regional tectonic inversion and strong crust-mantle interaction (Menzies and Xiu., 1998; Cai et al., 2013), which led to partial melting and dehydration of the lithospheric mantle and the lower crust as the temperature increased (Yang et al., 2003; Tan et al., 2015; Wen et al., 2015; Guo et al., 2020), and form a large-scale high heat flow, extensive crust-mantle mixture magmas. The magma migrated upward to the upper crust, subsequent magma mixing and the exsolved fluids extracted the ore-forming elements from the enclosing rocks to form the ore-forming fluids.

6 Conclusion

(1) The calcites which represent the main gold metallogenic stage (II) yielded a Sm-Nd isochron age of 123.5 ± 8.1 Ma (MSWD = 0.042). Subsequent geologic events were recorded by quartz diorite porphyrite dyke which are dated at 122.75 ± 0.66 Ma (MSWD = 1.5) by zircon LA-ICP-MS U-Pb dating. It is suggested that the Yangjiakuang gold mineralization took place in the early period of Early Cretaceous, which coincided with the first large-scale gold mineralization in the Jiaodong Peninsula.
(2) The S-Pb-He-Ar isotope compositions of pyrites in the Yangjiakuang gold deposit suggest that the ore-forming

materials and fluids are characterized by a mixture of crustal and mantle components.

(3) The gold mineralization is associated with extensional tectonic inversion caused by the rollback of the subducting Izanagi Plate during the early Cretaceous.

Data availability statement

The datasets presented in this study can be found in online repositories. The names of the repository/repositories and accession number(s) can be found in the article/Supplementary Material.

Author contributions

J-JL is the first corresponding author of this article, responsible for comprehensive technical guidance in the research process, comprehensively analyzed the test data and wrote the first draft of the article; Z-CD is the second corresponding author of this article. He participated in field investigation and sample collection, conducted surfer and lead isotope analysis and testing, and participated in the reviewing and finalizing the paper. CF carried out zircon U-Pb dating and participated in the revision of the manuscript. P-PZ, J-PT, and J-TH participated in sample collection and microscopic observation, data processing and isotope dating, and the revision of the manuscript. All authors contributed to the manuscript revision, read, and approved the submitted version.

Funding

The National Key Research and Development Program of China (Grant 2016YFC0600107) and projects from the China Geological Survey (Grants DD20190379-31, DD20221695-30 and 200110200038) support the financial of this work.

Acknowledgments

We thank the National Key Research and Development Program of China (Grant 2016YFC0600107) and projects from the China Geological Survey (Grants DD20190379-31, DD20221695-30 and 200110200038) for financial support for this work. The State Key Laboratory of Geological Processes and Mineral Resources [China University of Geosciences (Wuhan)], and the Beijing Institute of Geological Research of Nuclear Industry and Tianjin Center of China Geological Survey are thanked for supporting the laboratory analyses. We are grateful to Prof. Li Xiu-Zhang, Zhang Pi-Jian and Liao Xiao-Ming for field assistance and to Prof. Zhou Hong-Ying, Geng Jian-Zhen and Liu Wen-Gang for help with Sm-Nd and U-Pb isotopic dating.

Conflict of interest

The authors declare that the research was conducted in the absence of any commercial or financial relationships that could be construed as a potential conflict of interest.

Publisher's note

References

An, Y. (1990). A new division of the metamorphosed strata in the Jiaodong region and account on the newly delimited Jiaodong Group and Jingshan Group. *Shandong Geol.* 6, 97–103.

Andersen, T. (2002). Correction of common lead in U-Pb analyses that do not report ^{204}Pb. *Chem. Geol.* 1-2 (192), 59–79. doi:10.1016/s0009-2541(02)00195-x

Bell, K., Anglin, C. D., and Franklin, J. M. (1989). Sm-Nd and Rb-Sr isotope systematics of scheelites: Possible implications for the age and Genesis of vein-hosted gold deposits. *Geology* 17, 500–504. doi:10.1130/0091-7613(1989)017<0500:snarsi>2.3.co;2

Bendall, C., Lahaye, Y., Fiebig, J., Weyer, S., and Brey, G. P. (2006). *In situ* sulfur isotope analysis by laser ablation MC-ICPMS. *Appl. Geochem.* 21, 782–787. doi:10.1016/j.apgeochem.2006.02.012

Brugger, J., Maas, R., Lahaye, Y., McRae, C., Ghaderi, M., Costa, S., et al. (2002). Origins of Nd-Sr-Pb isotopic variations in single scheelite grains from Archaean gold deposits, Western Australia. *Chem. Geol.* 182, 203–225. doi:10.1016/s0009-2541(01)00290-x

Burnard, P. G., Hu, R. Z., Turner, G., and Bi, X. W. (1999). Mantle, crustal and atmospheric noble gases in Ailaoshan Gold deposits, Yunnan Province, China. *Geochim. Cosmochim. Acta* 63, 1595–1604. doi:10.1016/s0016-7037(99)00108-8

Cai, Y. C., Fan, H. R., Santosh, M., Liu, X., Hu, F. F., Yang, K. F., et al. (2013). Evolution of the lithospheric mantle beneath the southeastern North China craton: Constraints from mafic dikes in the Jiaobei terrain. *Gondwana Res.* 24, 601–621. doi:10.1016/j.gr.2012.11.013

Chen, J. F., Xie, Z., Li, H. M., Zhang, X. D., Zhou, T. X., Park, Y. S., et al. (2003). U-Pb zircon ages for a collision-related K-rich complex at Shidao in the Sulu ultrahigh pressure terrane, China. *Geochem. J.* 37, 35–46. doi:10.2343/geochemj.37.35

Chen, Y. J., Pirajno, F., and Qi, J. P. (2005). Origin of gold metallogeny and sources of ore-forming fluids, Jiaodong province, eastern China. *Ore Geol. Rev.* 47 (5), 530–549. doi:10.2747/0020-6814.47.5.530

Craddock, P. R., Rouxel, O. J., Ball, L. A., and Bach, W. (2008). Sulfur isotope measurement of sulfate and sulfide by high-resolution MC-ICP-MS. *Chem. Geol.* 253, 102–113. doi:10.1016/j.chemgeo.2008.04.017

Dang, Z. C., Li, J. J., Tian, J. P., He, J. T., Sun, Z. B., Tang, W. L., et al. (2022). Petrogenesis and geodynamic setting of the Late Jurassic Queshan adakitic granite, Jiaodong Peninsula, southeastern North China Craton: Zircon U-Pb geochronological, geochemical, and Lu-Hf isotopic evidence. *Geol. J.* 57 (5), 1891–1911. doi:10.1002/gj.4386

Deng, J., Liu, X. F., Wang, Q. F., and Pan, R. G. (2015). Origin of the jiaodong-type xinli gold deposit, Jiaodong Peninsula, China: Constraints from fluid inclusion and C-D-O-S-Sr isotope compositions. *Ore Geol. Rev.* 65, 674–686. doi:10.1016/j.oregeorev.2014.04.018

Deng, J., Qiu, K. F., Wang, Q. F., Goldfarb, R. J., Yang, L. Q., Zi, J. W., et al. (2020b). *In-situ* dating of hydrothermal monazite and implications on the geodynamic controls of ore formation in the Jiaodong gold province, eastern China. *Econ. Geol.* 115, 671–685. doi:10.5382/econgeo.4711

Deng, J., Wang, C. M., Bagas, L., Santosh, M., and Yao, E. Y. (2018). Crustal architecture and metallogenesis in the south-eastern North China Craton. *Earth-Science Rev.* 182, 251–272. doi:10.1016/j.earscirev.2018.05.001

Deng, J., Wang, Q. F., Santosh, M., Liu, X. F., Liang, Y. Y., Yang, L. Q., et al. (2020a). Remobilization of metasomatized mantle lithosphere: A new model for the Jiaodong gold province, eastern China. *Miner. Deposita* 55, 257–274. doi:10.1007/s00126-019-00925-0

Deng, J., Wang, Q. F., Wan, L., Liu, H., Yang, L. Q., and Zhang, J. (2011). A multifractal analysis of mineralization characteristics of the Dayingezhuang disseminated veinlet gold deposit in the Jiaodong gold province of China. *Ore Geol. Rev.* 40, 54–64. doi:10.1016/j.oregeorev.2011.05.001

Deng, J., Yang, L. Q., Ge, L. S., Wang, Q. F., Zhang, J., Gao, B. F., et al. (2006). Research advances in the Mesozoic tectonic regimes during the forming of Jiaodong ore cluster area. *Propress Nat. Sci.* 16 (8), 777–784. doi:10.1080/10020070612330069

Deng, J., Yang, L. Q., Groves, D. I., Zhang, L., Qiu, K. F., and Wang, Q. F. (2020c). An integrated mineral system model for the gold deposits of the giant Jiaodong province, eastern China. *Earth-Sciences Rev.* 208, 103274. doi:10.1016/j.earscirev.2020.103274

Ding, Z. J. (2014). *Study on metallogenic regularity of mesozoic precious and non-ferrous deposits in Jiaodong Peninsula: [Doctoral dissertation]*. Changchun: Jilin University.

Ding, Z. J., Sun, F. Y., Liu, F. L., Liu, J. H., Liu, D. H., Zhang, P. J., et al. (2013). U-Pb dating of zircons from the Weideshan molybdenum copper polymetallic deposits in Jiaodong Peninsula, China, and its geological significance. *Acta Petrol. Sin.* 29 (2), 607–618. doi:10.3724/SP.J.1008.2010.00937

Ding, Z. J., Sun, F. Y., Liu, F. L., Liu, J. H., Peng, Q. M., Ji, P., et al. (2015). Mesozoic geodynamic evolution and metallogenic series of major metal deposits in Jiaodong Peninsula. *Acta Petrol. Sin.* 31 (10), 3045–3080.

Fan, H. R., Hu, F. F., Yang, J. H., Shen, K., and Zhai, M. G. (2005). Fluid evolution and large-scale gold metallogeny during Mesozoic tectonic transition in the eastern Shandong province. *Acta Petrol. Sin.* 21 (5), 1317–1328.

Faure, M., Lin, W., Moni´ e, P., Le Breton, N., Poussineau, S., Panis, D., et al. (2003). Exhumation tectonics of the ultrahigh-pressure metamorphic rocks in the qinling orogen in east China: New petrological–structural–radiometric insights from the shandong Peninsula. *Tectonics* 22, 1018. doi:10.1029/2002tc001450

Guo, J. H., Chen, F. K., Zhang, X. M., Siebel, W., and Zhai, M. G. (2005). Evolution of syn-to post collisional magmatism from north Sulu UHP belt, eastern China: Zircon U-Pb geochronology. *Acta Petrol. Sin.* 21 (4), 1281–1301. doi:10.3321/j.issn:1000-0569.2005.04.025

Guo, L. N., Deng, J., Yang, L. Q., Wang, Z. L., Wang, S. R., Wei, Y. J., et al. (2020). Gold deposition and resource potential of the Linglong gold deposit, Jiaodong Peninsula: Geochemical comparison of ore fluids. *Ore Geol. Rev.* 120, 103434. doi:10.1016/j.oregeorev.2020.103434

Guo, L. N., Goldfarb, R. J., Wang, Z. L., Li, R. H., Chen, B. H., and Li, J. L. (2017). A comparison of Jiaojia- and Linglong-type gold deposit ore-forming fluids: Do they differ? *Ore Geol. Rev.* 88, 511–533. doi:10.1016/j.oregeorev.2016.12.003

Guo, P., Santosh, M., and Li, S. R. (2013). Geodynamics of gold metallogeny in the shandong province, NE China: An integrated geological, geophysical and geochemical perspective. *Gondwana Res.* 24 (3-4), 1172–1202. doi:10.1016/j.gr.2013.02.004

Hao, G. J., Wang, H. C., Niu, G. H., Kang, J. L., and Hao, S. (2020). Metamorphic geotectonic research and scientific in China. *Geol. Surv. Res.* 43 (2), 89–96.

Isozaki, Y. (1997). Permo-Triassic boundary superanoxia and stratified superocean: Records from lost deep sea. *Science* 276 (5310), 235–238. doi:10.1126/science.276.5310.235

Jackson, S. E., Pearson, N. J., Griffin, W. L., and Belousova, E. A. (2004). The application of laser ablation-inductively coupled plasma-mass spectrometry to *in situ* U-Pb zircon geochronology. *Chem. Geol.* 211 (1-2), 47–69. doi:10.1016/j.chemgeo.2004.06.017

Jahn, B. M., Liu, D. Y., Wan, Y. S., Song, B., and Wu, J. S. (2008). Archean crustal evolution of the Jiaodong Peninsula, China, as revealed by zircon SHRIMP geochronology, elemental and Nd-isotope geochemistry. *Am. J. Sci.* 308, 232–269. doi:10.2475/03.2008.03

Jiang, S. Y., Slack, J. F., and Palmer, M. R. (2000). Sm-Nd dating of the giant Sullivan Pb-Zn-Ag deposit, British Columbia. *Geology* 28, 751–754. doi:10.1130/0091-7613(2000)028<0751:sndotg>2.3.co;2

Kajiwara, Y., and Krouse, H. R. (1971). Sulfur isotope partitioning in metallic sulfide systems. *Can. J. Earth Sci.* 8, 1397–1408. doi:10.1139/e71-129

Kendrick, M. A., and Burnard, P. (2013). "Noble gases and halogens in fluid inclusions: A journey through the earth's crust," in *The noble gases as geochemical tracers* (Germany: Springer).

Li, G. H., Ding, Z. J., Song, M. C., Li, J. J., Li, X. Z., Ji, P., et al. (2017). The liaoshang pyrite–carbonate veined deposit: A new type of gold deposit in Jiaodong Peninsula. *Acta Geosci. Sin.* 38 (3), 423–429. doi:10.3975/cagsb.2017.03.12

Li, H. K., Geng, J. Z., Hao, S., Zhang, Y. Q., and Li, H. M. (2009). Study on the age of zircon U-Pb isotopes by laser ablation multi-receiver plasma mass spectrometer (LA-MC-ICPMS). *Acta Mineral. Sin.* 29 (S1), 600–601. doi:10.16461/j.cnki.1000-4734.2009.s1.014

Li, H., Sun, H. S., Evans, N. J., Li, J. W., Wu, J. H., Jiang, W. C., et al. (2019). Geochemistry and geochronology of zircons from granite-hosted gold mineralization in the Jiaodong Peninsula, North China: Implications for ore Genesis. *Ore Geol. Rev.* 115, 103188–103215. doi:10.1016/j.oregeorev.2019.103188

Li, J. J., Luo, Z. K., Liu, X. Y., Xu, W. D., and Luo, H. (2005). Geodynamic setting for formation of large-superlarge gold deposits and Mesozoic granites in Jiaodong area. *Mineral. Deposits* 24 (4), 361–372.

Li, J. J., Peng, Y., Zhang, T., Song, L. J., Ni, Z. P., Zhou, J. H., et al. (2021). Division of metallogenic units in North China. *North China Geol.* 44 (3), 4–24. doi:10.19948/j.12-1471/P.2021.03.02

Li, J. J., Zhang, P. P., Li, G. H., Liu, W. G., Zhao, Z. L., Li, X. Z., et al. (2020). Formation of the Liaoshang gold deposit, Jiaodong Peninsula, eastern China: Evidence from geochronology and geochemistry. *Geol. J.* 55 (8), 5903–5913. doi:10.1002/gj.3718

Li, J. W., Li, Z. K., Zhou, M. F., Chen, L., Bi, S. J., Deng, X. D., et al. (2012). The EarlyCretaceousYangzhaiyu lode gold deposit, north China craton: A link between craton reactivation and gold veining. *Econ. Geol.* 107, 43–79. doi:10.2113/econgeo.107.1.43

Li, J. W., Vasconcelos, P., Zhou, M. F., Zhao, X. F., and Ma, C. Q. (2006). Geochronology of the Pengjiakuang and rushan gold deposits, eastern Jiaodong gold province, northeastern China: Implications for regional mineralization and geodynamic setting. *Econ. Geol.* 101, 1023–1038. doi:10.2113/gsecongeo.101.5.1023

Li, K., Chen, Y., She, Z., Tang, H., and Chen, W. (2018). Carbon isotope compositions and geochemical characteristics of the Zhangshe graphite deposit of the Jingshan Group. *Jiaobei. Earth Sci. Front.* 25, 19–33. doi:10.13745/j.esf.sf.2018.4.11

Li, Q. L., Chen, F. K., Yang, J. H., and Fan, H. R. (2008). Single grain pyrite Rb-Sr dating of the Linglong gold deposit, eastern China. *Ore Geol. Rev.* 34, 263–270. doi:10.1016/j.oregeorev.2007.10.003

Li, S. R., and Santosh, M. (2017). Geodynamics of heterogeneous gold mineralization in the North China Craton and its relationship to lithospheric destruction. *Gondwana Res.* 50, 267–292. doi:10.1016/j.gr.2017.05.007

Li, Y. J., Li, S. R., Santosh, M., Liu, S. A., Zhang, L., Li, W. T., et al. (2015). Zircon geochronology, geochemistry and stable isotopes of the wang'ershan gold deposit, Jiaodong Peninsula, China. *Asian Earth Sci.* 113, 695–710. doi:10.1016/j.jseaes.2015.03.036

Liu, S. J., Jahn, B. M., Wan, Y. S., Xie, H. Q., Wang, S. J., Xie, S. W., et al. (2015). Neoarchean to Paleoproterozoic high-pressure mafic granulite from the Jiaodong Terrain, North China Craton: Petrology, zircon age determination and geological implications. *Gondwana Res.* 28, 493–508. doi:10.1016/j.gr.2014.07.006

Liu, W. G., Li, G. Z., Liu, H., and Li, H. M. (2018). Micro-fluorite sample digestion technology and high precision thermionic mass spectrometry determination for Sm-Nd isotopes. *Acta Geosci. Sin.* 39 (1), 119–124. doi:10.3975/cagsb.2017.122701

Liu, W. G., Liu, H., Li, G. Z., Zhou, H. Y., Xiao, Z. B., and Li, H. M. (2017). The application of ion exchange resins in Sr-Nd isotopic assay geological samples. *Acta Geol. Sin.* 91 (11), 2584–2592.

Liu, X. Y., Tan, J., He, H. Y., and Gan, J. G. (2021). Origin of the Tudui–Shawang gold deposit, Jiaodong Peninsula, north China Craton: Constraints from fluid inclusion and H-O-He-Ar-S-Pb isotopic compositions. *Ore Geol. Rev.* 133, 104125. doi:10.1016/j.oregeorev.2021.104125

Liu, Y., Deng, J., Wang, Z. L., Zhang, L., Zhang, C., Liu, X. D., et al. (2014). Zircon U-Pb ages, Lu-Hf isotopes and petrogeochemistry of the monzogranites from Xincheng gold deposit, northwestern Jiaodong Peninsula, China. *Acta Petrol.* 30 (9), 2559–2573.

Liu, Y., Gao, S., Hu, Z. C., Gao, C., and Wang, D. (2010). Continental and oceanic crust recycling-induced melt-peridotite interactions in the trans-north China orogen: U-Pb dating, Hf isotopes and trace elements in zircons from mantle xenoliths. *J. Petrology* 51 (1-2), 537–571. doi:10.1093/petrology/egp082

Liu, Z. K., Hollings, P., Mao, X. C., Christopher, J. M., Yang, B., and Lei, T. (2021). Metal remobilization from country rocks into the Jiaodong-type orogenic gold systems, Eastern China: New constraints from scheelite and galena isotope results at the Xiadian and Majiayao gold deposits. *Ore Geol. Rev.* 134, 104126. doi:10.1016/j.oregeorev.2021.104126

Ludwig, K. R. (2003). "User's manual for isoplot/ex version 3.00: A geochronological toolkit for microsoft excel," in *Berkeley geochronology center special publication No.* (Berkeley CA: World Cat).

Luo, Z. K., and Miao, L. C. (2002). *Granite and gold deposits in Zhaolai area, Jiaodong region*. Beijing: Metallurgical Industy Press.

Ma, L., Jiang, S. Y., Dai, B. Z., Jiang, Y. H., Hou, M. L., Pu, W., et al. (2013). Multiple sources for the origin of Late Jurassic Linglong adakitic granite in the Shandong Peninsula, eastern China: Zircon U-Pb geochronological, geochemical and Sr-Nd-Hf isotopic evidence. *Lithos* 162-163, 251–263. doi:10.1016/j.lithos.2013.01.009

Mamyrin, B. A., and Tolstikhin, I. N. (1984). *Helium isotopes in nature*. Amsterdam: Elsevier.

Mao, J. W., Wang, Y. T., Li, H. M., Pirajno, F., Zhang, C. Q., and Wang, R. T. (2008). The relationship of mantle-derived fluids to gold metallogenesis in the Jiaodong Peninsula: Evidence from D-O-C-S isotope systematics. *Ore Geol. Rev.* 33, 361–381. doi:10.1016/j.oregeorev.2007.01.003

Maruyama, S., Isozaki, Y., Kimura, G., and Terabayashi, M. (1997). Paleogeographic maps of the Japanese islands: Plate tectonic synthesis from 750 Ma to the present. *Isl. Arc* 6 (1), 121–142. doi:10.1111/j.1440-1738.1997.tb00043.x

Menzies, M. A., and Xu, Y. G. (1998). "Geodynamics of the North China craton," in *Mantle dynamics and plate interactions in east asia* (United States: American Geophysical Union).

Ohmoto, H. (1972). Systematics of sulfur and carbon isotopes in hydrothermal ore deposits. *Econ. Geol.* 67, 551–578. doi:10.2113/gsecongeo.67.5.551

Peng, J. T., Zhang, D. L., Hu, R. Z., Wu, M. J., and Lin, Y. X. (2008). Sm-Nd and Sr isotope geochemistry of hydrothermal scheelite from the Zhazixi W-Sb deposit, Western Hunan. *Acta Geol. Sin.* 82 (11), 1514–1521.

Qiu, L. G., Ren, F. L., Cao, Z. X., and Zhang, Y. Q. (2008). Late Mesozoic magmatic activities and their constraints on geotectonics of Jiaodong region. *Geotect. Metallogenia* 32 (1), 117–123. doi:10.16539/j.ddgzyckx.2008.01.003

Saravanan, C. S., and Mishra, B. (2009). Uniformity in sulfur isotope composition in the orogenic gold deposits from the Dharwar Craton, southern India. *Min. Deposita* 44, 597–605. doi:10.1007/s00126-009-0241-7

Song, M. C., Li, J., Yu, X. F., Song, Y. X., Ding, Z. J., and Li, S. Y. (2021). Metallogenic characteristics and tectonic setting of the Jiaodong gold deposit, China. *Solid Earth Sci.* 6, 385–405. doi:10.1016/j.sesci.2021.07.002

Song, M. C., Song, Y. X., Li, J., and Li, S. Y. (2015). Metallogenic series of gold and nonferrous metal deposits related tocretaceous granites in eastern Shandong Peninsula. *Geotect. Metallogenia* 39 (5), 828–843. doi:10.16539/j.ddgzyckx.2015.05.007

Song, M. C., Zhou, J. B., Song, Y. X., Wang, B., Li, S. Y., Li, J., et al. (2020). Mesozoic Weideshan granitoid suite and its relationship to large-scale gold mineralization in the Jiaodong Peninsula, China. *Geol. J.* 55, 5703–5724. doi:10.1002/gj.3607

Stuart, F. M., Burnard, P. G., Taylor, R. P., and Turner, G. (1995). Resolving mantle and crustal contributions to ancient hydrothermal fluids: He-Ar isotopes in fluid inclusions from DaeHwa W-Mo mineralisation, South Korea. *Geochim. Cosmochim. Acta* 59, 4663–4673. doi:10.1016/0016-7037(95)00300-2

Tan, J., Wei, J. H., Li, Y. J., Fu, L. B., Li, H. M., Shi, W. J., et al. (2015). Origin and geodynamic significance of fault-hosted massive sulfide gold deposits from the guocheng-liaoshang metallogenic belt, eastern Jiaodong Peninsula: Rb-Sr dating, and H-O-S-Pb isotopic constraints. *Ore Geol. Rev.* 65, 687–700. doi:10.1016/j.oregeorev.2014.06.007

Tang, J., Zheng, Y. F., Wu, Y. B., Gong, B., and Liu, X. M. (2007). Geochronology and geochemistry of metamorphic rocks in the Jiaobei terrane: Constraints on its tectonic affinity in the Sulu orogen. *Precambrian Res.* 152 (1), 48–82. doi:10.1016/j.precamres.2006.09.001

Tian, J. P., Li, J. J., Zhang, P. P., Li, X. Z., Liu, W. G., Tang, W. L., et al. (2020). Formation of the Majiayao gold deposit, Jiaodong Peninsula, eastern China: Constraints from fluid inclusions, H-O-S-Pb isotopes, and pyrite Rb-Sr age. *Geol. J.* 55 (8), 5885–5902. doi:10.1002/gj.3719

Tian, R. C., Li, D. P., Tian, J. P., Yu, X. W., Zhang, W., Zhu, P. G., et al. (2022). Genesis of the Jiudian gold deposit, Jiaodong Peninsula, eastern China: Fluid inclusion and C-H-O-Pb isotope constraints. *Ore Geol. Rev.* 149, 105086. doi:10.1016/j.oregeorev.2022.105086

Turner, G., Burnard, P., Ford, J. L., Gilmour, J. D., Lyon, I. C., and Stuart, F. M. (1993). Tracing fluid sources and interactions. *Phil. Trans. R. Soc. Lond. A* 344, 127–140.

Wang, B., Song, M. C., Zhou, J. B., and Ding, Z. J. (2022). Four stages A-type granitoids in Shandong Province and their implications for tectonic evolution. *North China Geol.* 45 (2), 1–17.

Wang, G. Q. (2016). *Mineralization of the Xincheng gold deposit, northwest Jiaodong Peninsula: Multiple isotope tracer*. Beijing: China University of Geosciences.

Wang, J. N., Qu, H. F., and Sun, Z. W. (2017). Geological charteristics of Yangjiakuang gold deposit and prospecting. *Inn. Mong. Sci. Technol. Econ.* 387 (17), 51–53.

Wang, S. J., Wan, Y. S., Zhang, C. J., Yang, E. X., Song, Z. Y., Wang, L. F., et al. (2009). Forming ages of early precambrian metamorphic strata in shandong province—Proofs of zircon SHRIMP U-Pb dating. *Shandong Land Resour.* 25, 18–24.

Wang, Z. L., Zhao, R. X., Zhang, Q., Lu, H. W., Li, L., and Cheng, W. (2014). Magma mixing for the high Ba-Sr guojialing-type granitoids in northwest Jiaodong Peninsula: Constraints from petrogeochemistry and Sr-Nd isotopes. *Acta Petrol. Sin.* 30 (9), 2595–2608.

Wen, B. J., Fan, H. R., Santosh, M., Hu, F. F., Pirajno, F., and Yang, K. F. (2015). Genesis of two different types of gold mineralization in the Linglong gold field, China: Constrains from geology, fluid inclusions and stable isotope. *Ore Geol. Rev.* 65, 643–658. doi:10.1016/j.oregeorev.2014.03.018

Wu, F. Y., Lin, J. Q., Wilde, S. A., Zhang, X. O., and Yang, J. H. (2005). Nature and significance of the early cretaceous giant igneous event in eastern China. *Earth Planet. Sci. Lett.* 233, 103–119. doi:10.1016/j.epsl.2005.02.019

Wu, J. H., Chen, Y. L., Zheng, C. Y., Li, H., Yong, Z. K., Tang, Y. Y., et al. (2021). Genesis of the Longkou–Tudui gold deposit, Jiaodong Peninsula, eastern China: Constraints from zircon U-Pb dating, fluid inclusion studies and C-H-O-S stable isotopes. *Ore Geol. Rev.* 139, 104449. doi:10.1016/j.oregeorev.2021.104449

Xie, S. W., Wang, S. J., Xie, H. Q., Liu, S. J., Dong, C. Y., Ma, M. Z., et al. (2015). Petrogenesis of ca. 2.7 Ga TTG rocks in the Jiaodong terrane, North China craton and its geological implications. *Acta Petrol. Sin.* 31 (10), 2974–2990.

Xie, S. W., Xie, H. Q., Wang, S. J., Krönera, A., Liu, S. J., Zhou, H. Y., et al. (2014). Ca.2.9 Ga granitoid magmatism in eastern Shandong, North China Craton: Zircon dating, Hf-in-zircon isotopic analysis and whole-rock geochemistry. *Precambrian Res.* 255, 538–562. doi:10.1016/j.precamres.2014.09.006

Xu, Y., Mao, G., Liu, X., An, P., Wang, Y., and Cao, M. (2022a). Genesis of the zhaoxian gold deposit, Jiaodong Peninsula, China: Insights from *in-situ* pyrite geochemistry and S-He-Ar isotopes, and zircon U-Pb geochronology. *Front. Earth Sci.* 10, 886975. doi:10.3389/feart.2022.886975

Xu, Y. W., Mao, G. Z., Liu, X. T., An, P. R., Wang, Y., and Cao, M. P. (2022b). Genesis of the zhaoxian gold deposit, Jiaodong Peninsula, China: Insights from *in-situ* pyrite geochemistry and S-He-Ar isotopes, and zircon U-Pb geochronology. *Front. Earth Sci.* 10. doi:10.3389/feart.2022.886975

Yang, J. H., Chung, S. L., Wilde, S. A., Wu, F. Y., Chu, M. F., Lo, C. H., et al. (2005). Petrogenesis of post-orogenic syenites in the Sulu orogenic belt, east China: Geochronological, geochemical and Nd-Sr isotopic evidence. *Chem. Geol.* 214, 99–125. doi:10.1016/j.chemgeo.2004.08.053

Yang, J. H., Wu, F. Y., and Wilde, S. A. (2003). A review of the geodynamic setting of large-scale late mesozoic gold mineralization in the North China craton: An association with lithospheric thinning. *Ore Geol. Rev.* 23, 125–152. doi:10.1016/s0169-1368(03)00033-7

Yang, J. H., and Zhou, X. H. (2001). Rb-Sr, Sm-Nd, and Pb isotope systematics of pyrite: Implications for the age and Genesis of lode gold deposits. *Geology* 29, 711–714. doi:10.1130/0091-7613(2001)029<0711:rssnap>2.0.co;2

Yang, K. F., Fan, H. R., Santosh, M., Hu, F. F., Wilde, S. A., Lan, T. G., et al. (2012). Reactivation of the Archean lower crust: Implications for zircon geochronology, elemental and Sr–Nd–Hf isotopic geochemistry of late Mesozoic granitoids from northwestern Jiaodong Terrane, the North China Craton. *Lithos* 146, 112–127. doi:10.1016/j.lithos.2012.04.035

Yang, L. Q., Deng, J., Goldfarb, R. J., Zhang, J., Gao, B. F., and Wang, Z. L. (2014b). $^{40}Ar/^{39}Ar$ geochronological constraints on the formation of the Dayingezhuang gold deposit: New implications for timing and duration of hydrothermal activity in the Jiaodong gold province, China. *Gondwana Res.* 25, 1469–1483. doi:10.1016/j.gr.2013.07.001

Yang, L. Q., Deng, J., Wang, Z. L., Zhang, L., Guo, L. N., Song, M. C., et al. (2014a). Mesozoic gold metallogenic system of the Jiaodong gold province, eastern China. *Acta Pet. Sin.* 30, 2447–2467.

Yang, W., and Li, S. (2008). Geochronology and geochemistry of the mesozoic volcanic rocks in western liaoning: Implications for lithospheric thinning of the North China craton. *Lithos* 102, 88–117. doi:10.1016/j.lithos.2007.09.018

Yu, P. X., Xiao, X., Xie, J. M., Zhao, Y. B., Liu, D. S., and Shi, H. J. (2014). Analysis on geological and ore controlling conditions of Yangjiakuang gold deposit in Qixia city of shandong province. *Shandong Land Resour.* 30 (9), 7–9.

Yuan, Z. Z., Li, Z. K., Zhao, X. F., Sun, H. S., Qiu, H. N., and Li, J. W. (2019). New constraints on the Genesis of the giant Dayingezhuang gold (silver) deposit in the Jiaodong district, North China Craton. *Ore Geol. Rev.* 112, 103038. doi:10.1016/j.oregeorev.2019.103038

Zartman, R., and Doe, B. (1981). Plumbotectonics—The model. *Tectonophysics* 75, 135–162. doi:10.1016/0040-1951(81)90213-4

Zhai, M. G., Fan, H. R., Yang, J. H., and Miao, L. C. (2004). Large-scale cluster of gold deposits in east shandong: Anorogenic metallogenesis. *Earth Sci. Front.* 11 (1), 85–98.

Zhai, M. G., and Santosh, M. (2013). Metallogeny of the North China craton: Link with secular changes in the evolving earth. *Gondwana Res.* 24, 275–297. doi:10.1016/j.gr.2013.02.007

Zhang, F. X., Xiao, L., and Qi, Y. L. (2004). Exploration and study of Carlin and Carlin-like type gold deposits: Review and prospect. *Geol. China* 04, 406–412.

Zhang, H. Y., Blenkinsop, T., and Yu, Z. W. (2020). Timing of Triassic tectonic division and postcollisional extension in the eastern part of the Jiaodong Peninsula. *Gondwana Res.* 83, 141–156. doi:10.1016/j.gr.2020.01.018

Zhang, J., Zhao, Z. F., Zheng, Y. F., and Dai, M. (2010). Postcollisional magmatism: Geochemical constraints on the petrogenesis of Mesozoic granitoids in the Sulu orogen, China. *Lithos* 119, 512–536. doi:10.1016/j.lithos.2010.08.005

Zhang, L. C., Liu, T. B., Shen, Y. C., Zeng, Q. D., and Li, G. M. (2003). Structure, isotopes, and $^{40}Ar/^{39}$ Ar dating of the Pengjiakuang gold deposit, Mesozoic Jiaolai basin, eastern China. *Int. Geol. Rev.* 45, 691–711. doi:10.2747/0020-6814.45.8.691

Zhang, L., Weinberg, R. F., Yang, L. Q., Groves, D. I., Sai, S. X., Matchan, E., et al. (2020). Mesozoic orogenic gold mineralization in the Jiaodong Peninsula, China: A focused event at 120 ± 2 Ma during cooling of pregold granite intrusions. *Econ. Geol.* 115, 415–441. doi:10.5382/econgeo.4716

Zhang, P. P. (2018). *Study on the mineralization of gold deposits in the guocheng district, Jiaodong: [Master dissertation]*. Tianjin: Sinosteel Tianjin Geological Academy Co., Ltd.

Zhang, T., and Zhang, Y. Q. (2007). Geochronological sequence of Mesozoic intrusive magmatism in Jiaodong Peninsula and its tectonic constraints. *Geol. J. China Univ.* 13 (2), 323–336.

Zhao, G. C., and Zhai, M. G. (2013). Lithotectonic elements of precambrian basement in the North China craton: Review and tectonic implications. *Gondwana Res.* 23, 1207–1240. doi:10.1016/j.gr.2012.08.016

Zhao, K. D., and Jiang, S. Y. (2004). Direct isotope dating for metallic ore deposits. *Earth Sci. Front.* 11 (2), 425–434.

Zhao, R., Wang, Q. F., Deng, J., Santosh, M., Liu, X. F., and Cheng, H. Y. (2018). Late mesozoic magmatism and sedimentation in the Jiaodong Peninsula: New constraints on lithospheric thinning of the North China craton. *Lithos* 322, 312–324. doi:10.1016/j.lithos.2018.10.020

Zhu, G., Liu, C., Gu, C., Zhang, S., Li, Y., Su, N., et al. (2018). Oceanic plate subduction history in the Western pacific ocean: Constraint from late mesozoic evolution of the tan-Lu fault zone. *Sci. China Earth Sci.* 61 (4), 386–405. doi:10.1007/s11430-017-9136-4

Zhu, R. X., Fan, H. R., Li, J. W., Meng, Q. R., Li, S. R., and Zeng, Q. D. (2015). Decratonic gold deposits. *Sci. China Earth Sci.* 45 (8), 1523–1537. doi:10.1007/s11430-015-5139-x